N94-30619

209926
p. 27

Dynamic Constraints on CO_2 Uptake by an Iron-Fertilized Antarctic

Tsung-Hung Peng, W.S. Broecker, and H.G. Östlund[1]

Introduction

Because of the concern regarding the impacts of greenhouse warming caused by rising atmospheric CO_2 content, consideration is being given to the possibility that the power of the ocean's biological carbon pump could be artificially strengthened. The linkage between atmospheric CO_2 and marine biological activity is the gas exchange across the sea-air interface and photosynthesis in the photic zone of the surface waters. The organic material formed in surface water would take up about 130 carbon atoms per phosphorus atom. Thus the effect of biological activity is to reduce the total CO_2 (ΣCO_2) content in the surface water. The CO_2 partial pressure (pCO_2) in surface ocean water is influenced, in turn, by the extent to which photosynthesis reduces the ΣCO_2 content of the water. The magnitude of this reduction is controlled by the efficiency with which the limiting nutrients phosphorus tetroxide or phosphate (PO_4) and nitrogen trioxide or nitrate (NO_3) are utilized. In temperate and tropical oceans the utilization efficiency is high, and hence pCO_2 reduction is close to maximum. By contrast, in the polar oceans the utilization efficiency is low, leaving plenty of nutrients unused. Therefore, if a way can be found to increase the efficiency of

[1]This chapter has been authorized by a contractor of the U.S. government under contract DE-AC05-84OR21400. Accordingly, the U.S. government retains a nonexclusive, royalty-free license to publish or reproduce the published form of this contribution, or allow others to do so, for U.S. government purposes.

nutrient utilization in these waters, their pCO_2 and in turn that for the atmosphere could be reduced.

Recently (Martin, 1990; Martin et al., 1990b; Baum, 1990), iron fertilization in the Antarctic has been proposed as a potential means to enhance the biological carbon pump for drawing down pCO_2 in this region and hence to absorb more CO_2 from the atmosphere to reduce the rising atmospheric CO_2. Martin and his co-workers (Martin and Fitzwater, 1988; Martin and Gordon, 1988; Martin et al., 1989, 1990a, 1990b; Martin, 1990) have shown in incubation experiments that plant growth rates in waters from polar regions can be accelerated through the addition of trace amounts of dissolved iron. Iron is an essential micronutrient required for the metabolism of all forms of life. Its primary function is in cytochrome formation. Because iron is one of the most particle-reactive elements, its concentration in the sea is very low, with the lowest values occurring in regions like the Antarctic which are most remote from the continental sources.

Extensive discussion and consideration have been given to the biological aspects of Martin's iron fertilization hypothesis. However, very little attention has been directed to the potential dynamic constraints on CO_2 uptake resulting from the enhanced biological carbon pump in the Antarctic. Through discussion with J. Sarmiento, we became interested in studying the response of atmospheric CO_2 to a successful iron fertilization in the Antarctic. Our major concern is the limitation by ocean dynamics of the potential for CO_2 removal. We present here a tracer-calibrated advection-diffusion box model which incorporates the rate at which surface waters in the Antarctic Ocean are replaced by vertical mixing and advection. This replacement process governs the rate of CO_2 removal from the atmosphere.

In a hypothetical case where water circulation does not exist in the Antarctic ocean, only an amount of CO_2 equivalent to that removed as a result of the initial iron fertilization would be sequestered from the atmosphere. In such a situation the atmosphere and surface oceans of Antarctic and non-Antarctic regions would rapidly reach a new equilibrium, leaving the atmosphere with a CO_2 content only slightly lower than it had before iron fertilization was instituted. In order to achieve a significant reduction of the atmosphere's CO_2 content, the surface waters of the Antarctic must be replaced frequently from below. Thus, the critical issue is the rate of vertical mixing in the Antarctic ocean.

Tracer Distribution and Dynamics in the Antarctic Ocean

The distribution of anthropogenic tracers in the Antarctic provides important constraints regarding the surface water replacement

rate. Measurements made as part of the Geochemical Ocean Sections Survey (GEOSECS) program (see Figure 1 for station locations) provided the basic data. The first piece of information these results supply is geographic domain in which surface waters contain appreciable amounts of unused NO_3 and PO_4. As can be seen from the map in Figure 1, the ambient PO_4 level for Antarctic surface water (during the summer months) of 1.6 μmol drops off rapidly between 50°S and 40°S. We adopted 45°S to be the northern boundary of the region where iron fertilization has potential. Table 1 shows the area of the ocean in 5° latitude belts south of this boundary. The total represents 16.8% of the global ocean.

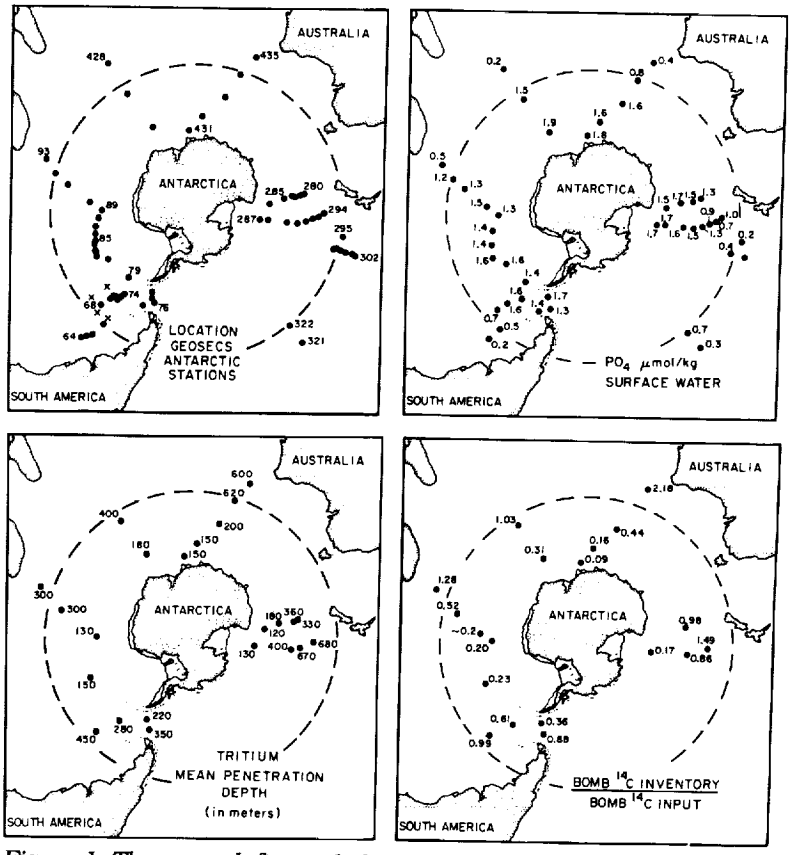

Figure 1. The upper left panel shows the location of the GEOSECS Antarctic stations (black dots) and of four SAVE stations (crosses). The other three maps show the surface water PO_4 concentrations at these stations, the mean penetration depth of tritium at the time of the GEOSECS surveys (see Broecker et al., 1986), and the ratio of the water column inventory of nuclear testing radiocarbon to the input of nuclear testing radiocarbon (see Broecker et al., 1985). The dashed circle at 45°S marks the latitude where, on the average, surface PO_4 reaches one-half its ambient Antarctic concentration.

Table 1: Ocean areas in 5° latitude belts for the Antarctic region

Latitude Range	Area (10^6 km^2)	% of Global Ocean Area
80°S–75°S	0.52	0.1
75°S–70°S	2.60	0.7
70°S–65°S	6.82	1.9
65°S–60°S	10.30	2.9
60°S–55°S	12.01	3.3
55°S–50°S	13.89	3.8
50°S–45°S	14.69	4.1
Total	60.83	16.8

From Sverdrup et al., 1942.

The results of the tritium (^{3}H), carbon-14 (^{14}C), and silica (SiO_2) measurements for Southern Ocean stations are summarized in Figure 2. Two aspects are important. First, the tritium results allow an estimate to be made of the extent of downward mixing into the thermocline on the time scale of one decade (i.e., the time between the tritium delivery and the GEOSECS surveys). As can be seen from the summary in Figure 1, this depth ranges from as little as 150 m in the deep Antarctic to as much as 600 m at 45°S. Second, as the tritium profile at any given station is the mirror image of the dissolved silica profile, the far more complete silica data set can be used to portray the upper ocean volume available for the uptake of

(text continues on p. 84)

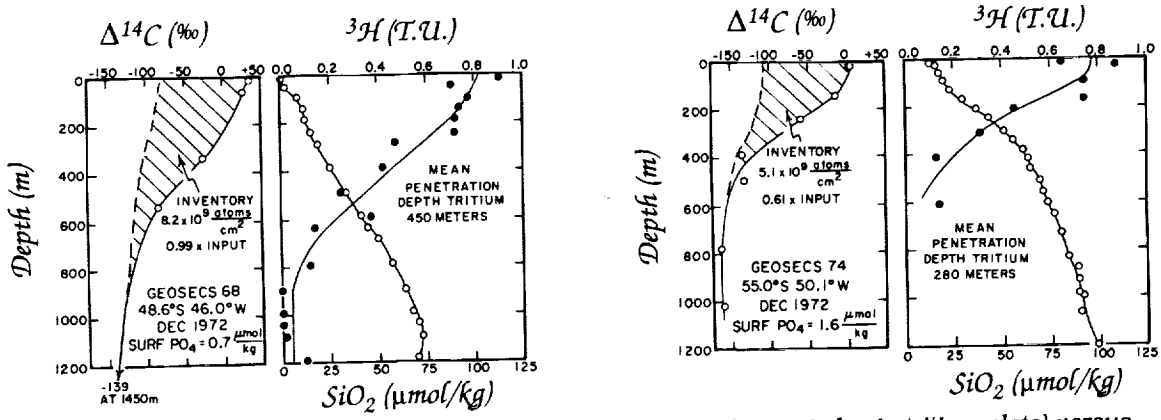

Figure 2. Plots of radiocarbon, tritium (solid circles), and silica (open circles in tritium plots) versus depth for 24 stations occupied during the GEOSECS program. Following Broecker et al. (1985), an estimate of the prenuclear radiocarbon profile is reconstructed, allowing the inventory of bomb ^{14}C (cross-hatched sections) to be calculated. The error of individual tritium measurements ranges from 0.5 T.U. for the Indian Ocean stations to 0.9 T.U. for the Atlantic and Pacific stations. The data are from Östlund and Stuiver, 1980; Stuiver and Östlund, 1980; Stuiver and Östlund, 1983; and the GEOSECS atlas series.

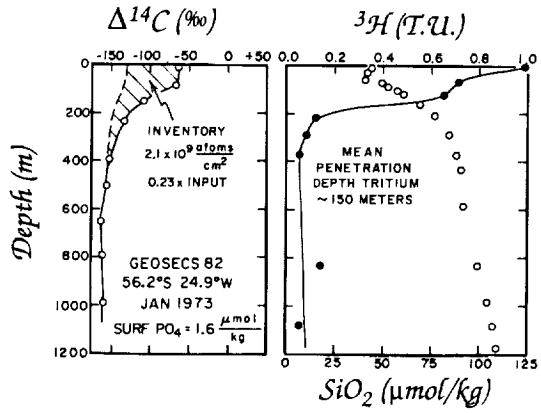

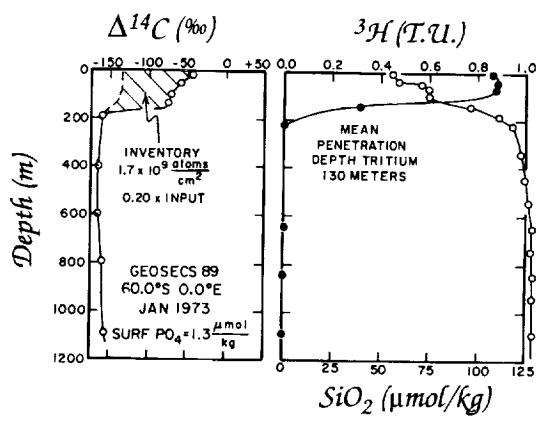

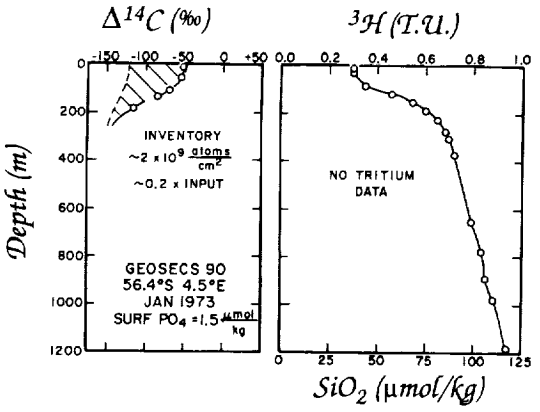

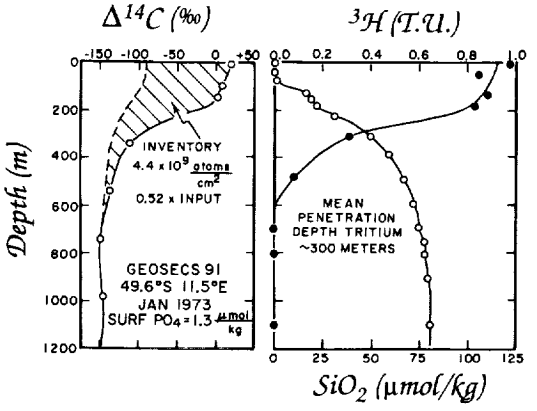

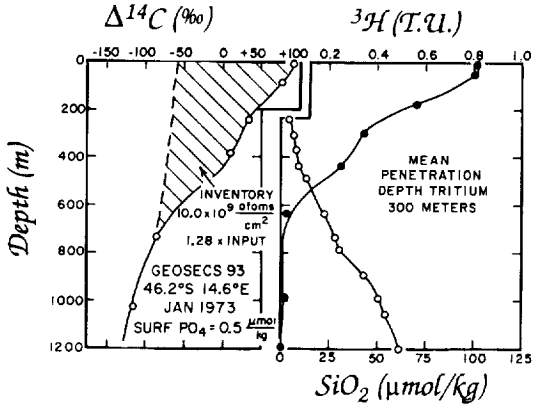

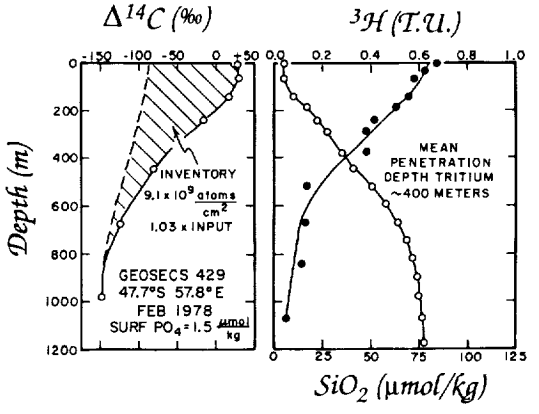

Figure 2, continued.

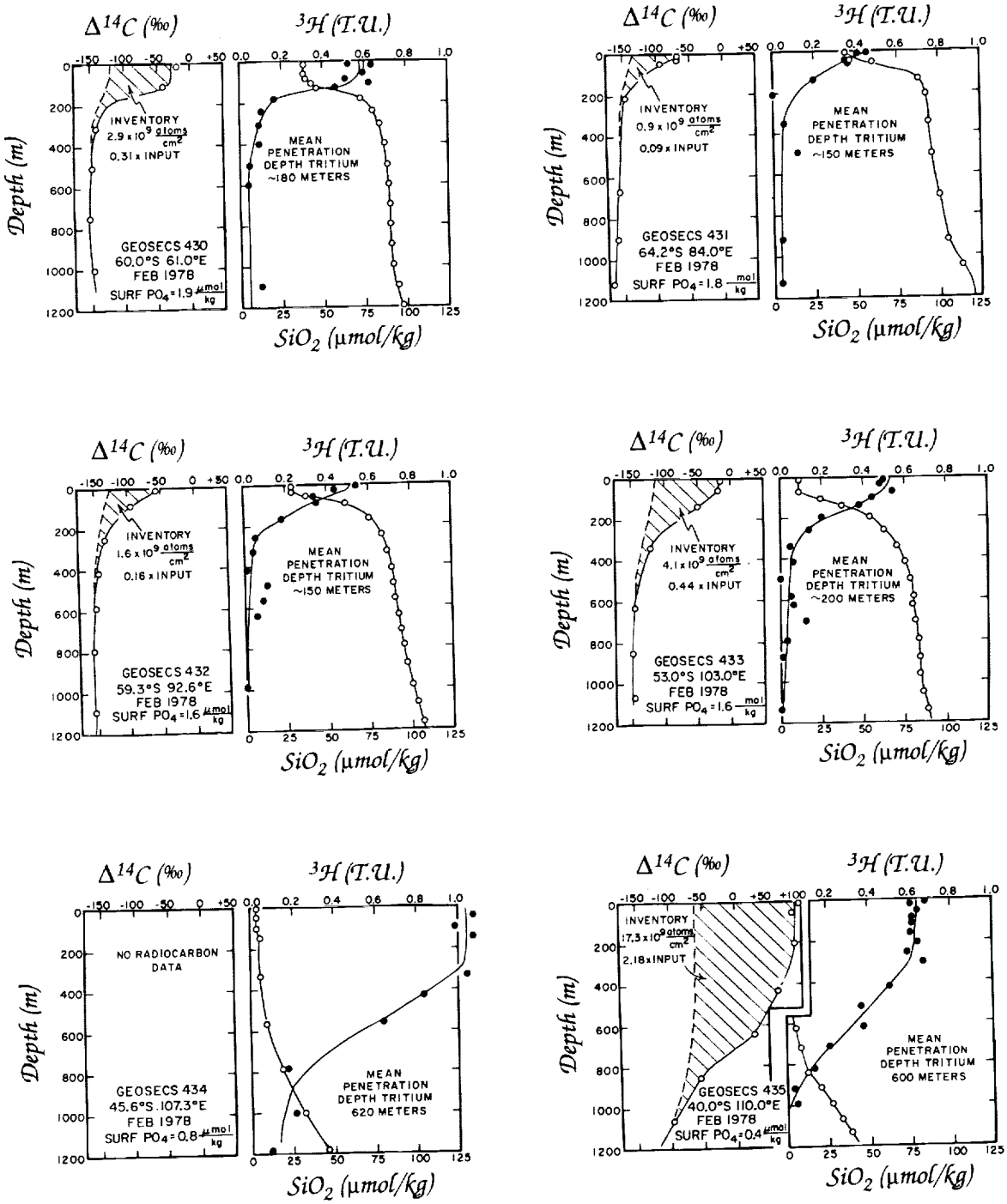

Figure 2, continued.

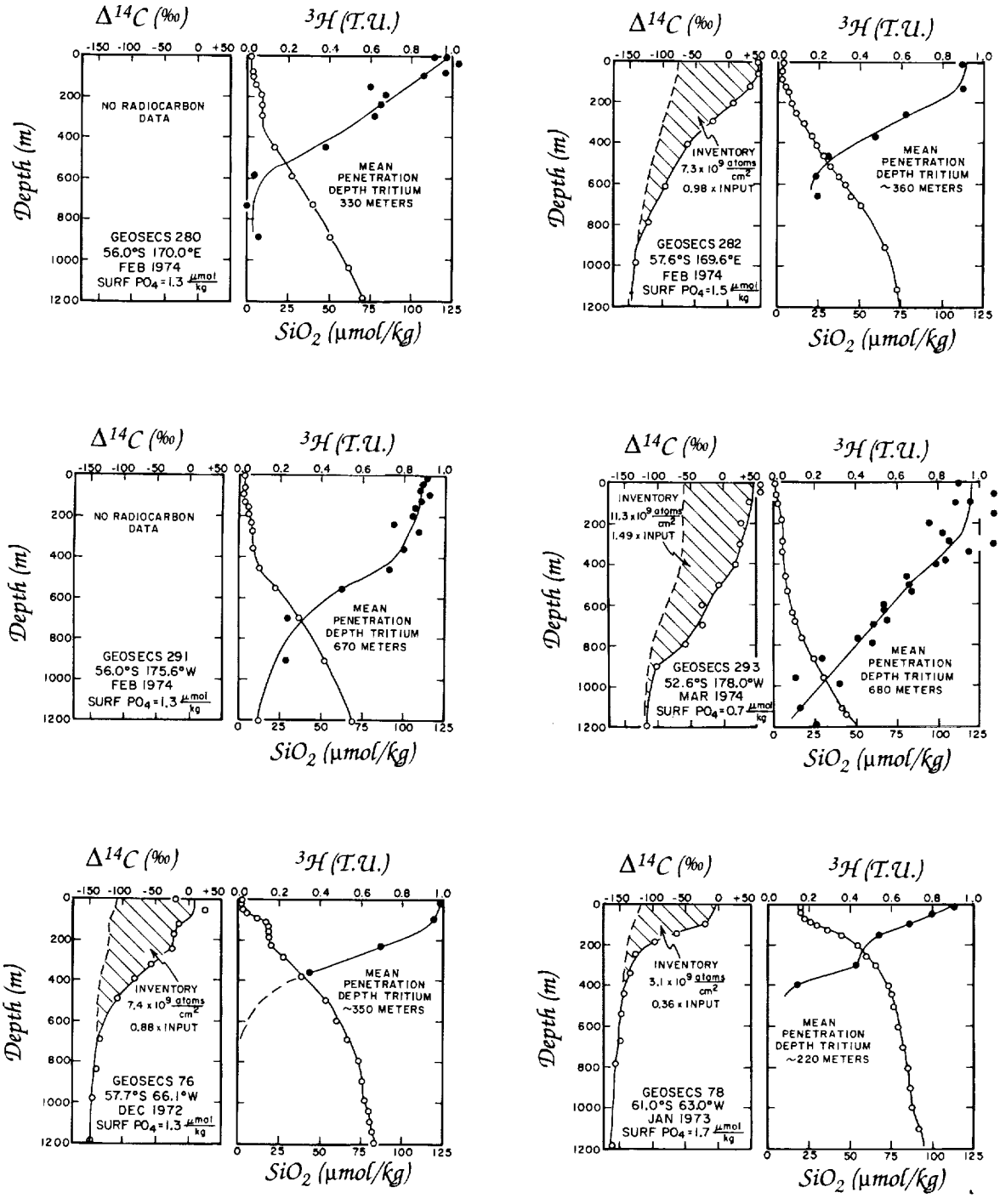

Figure 2, continued.

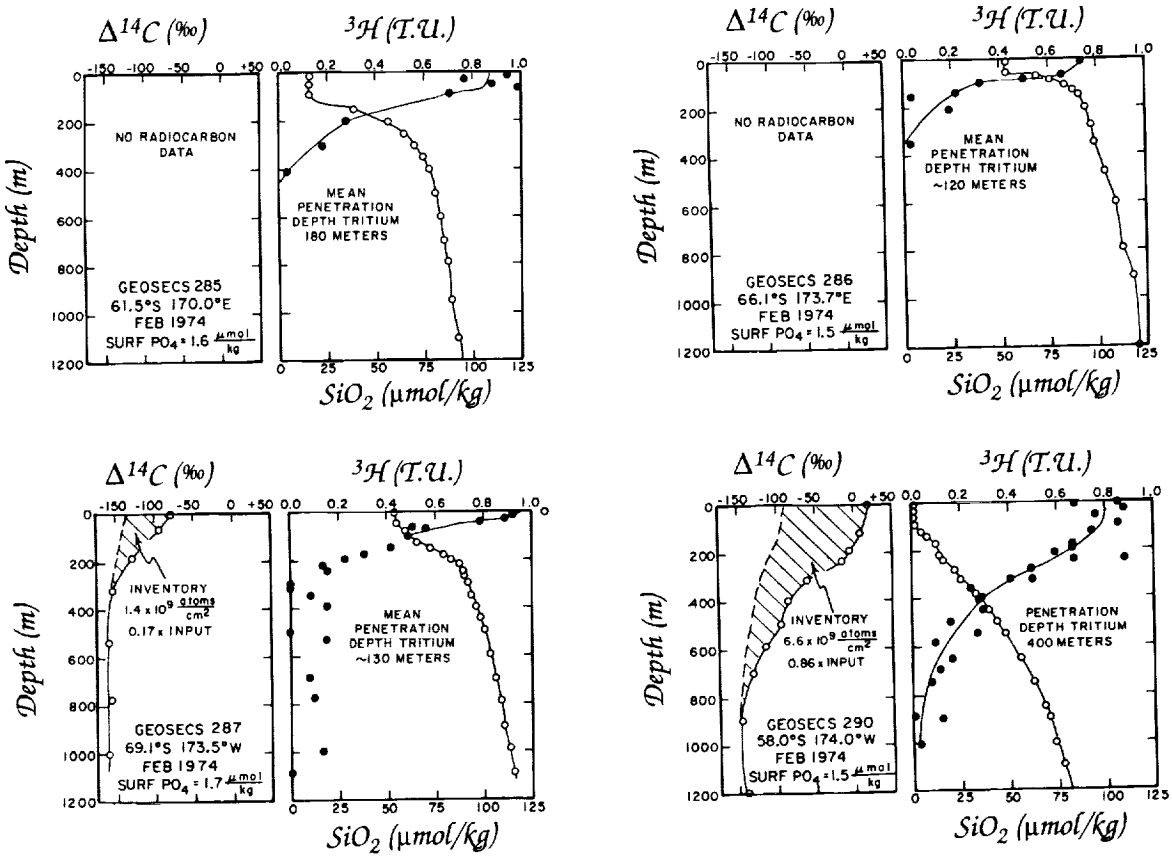

Figure 2, continued.

excess CO_2 on the time scale of one decade. Figure 3 summarizes meridional sections of dissolved silica for the Antarctic.

The other important source of information comes from the ^{14}C results. Broecker et al. (1985) used measurements on samples taken before the above-ground nuclear testing of the 1950s to estimate the prenuclear $\Delta^{14}C$ values for surface waters at the GEOSECS stations at which ^{14}C measurements were made. The ^{3}H measurements allowed an estimate to be made of the depth to which significant amounts of bomb-produced ^{14}C had penetrated at the time of the GEOSECS surveys. With these two end points and a knowledge of the shape of the ^{3}H profile, the prenuclear ^{14}C profile for each station could be established. The area between the measured profile and the prenuclear profile provided an estimate of the water column burden of excess ^{14}C. Broecker et al. (1985) showed that these excesses have a distinct geographic pattern (see Figure 4). Higher-than-average inventories are found in the temperate regions of the ocean and in the northern Atlantic. Lower-than-aver-

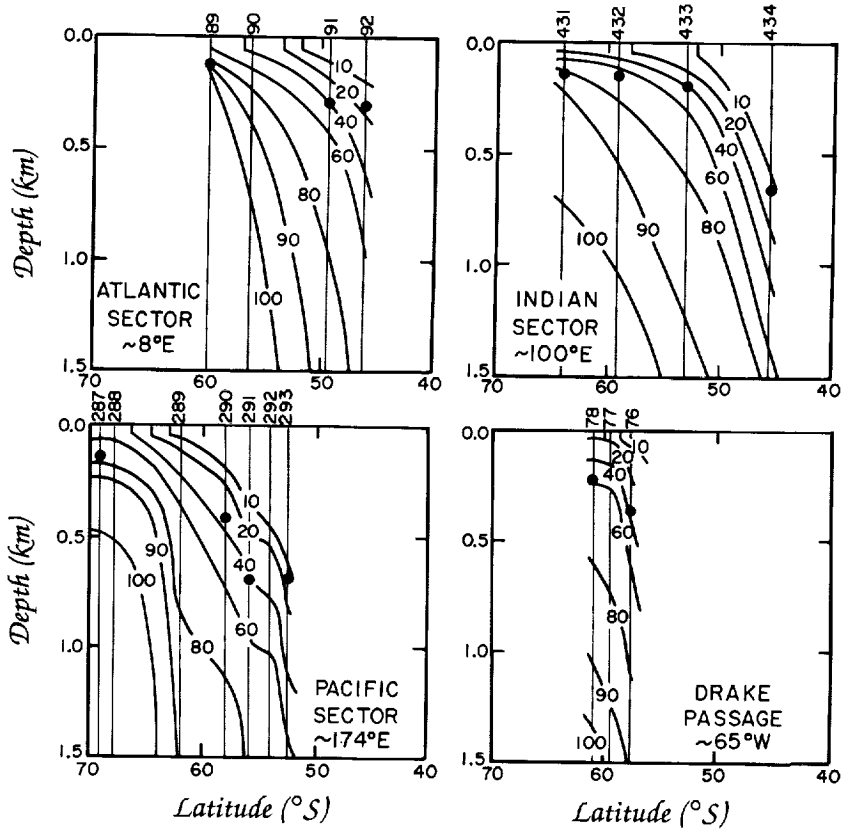

Figure 3. Meridional sections of dissolved silica (μmol/kg) for the Antarctic. At the time of the GEOSECS survey an excellent anticorrelation existed between tritium and silica for each station (see Figure 2). The large dots show the mean penetration depth of tritium for those stations (numbers on top axis) where tritium measurements were made. This diagram provides a feeling for the geometry of the volume available for excess CO_2 storage.

age inventories are found in the equatorial zone, in the northern Pacific, and in the Southern Ocean. These authors pointed out that the areas of high inventory correspond to regions of downwelling and the areas of low inventory to regions of upwelling. Further, they attributed this correspondence to lateral transport of bomb-produced ^{14}C from regions of upwelling to regions of downwelling. Experiments conducted with the Geophysical Fluid Dynamics Laboratory ocean model confirmed that such transports can explain the inventory pattern (Toggweiler et al., 1989).

Broecker et al. (1985) went a step further and compared the inventory at any given station to the net amount of bomb-produced ^{14}C invading that station from the atmosphere. This allowed the magnitude of the excess or deficiency to be quantified (see Figure 5). Their

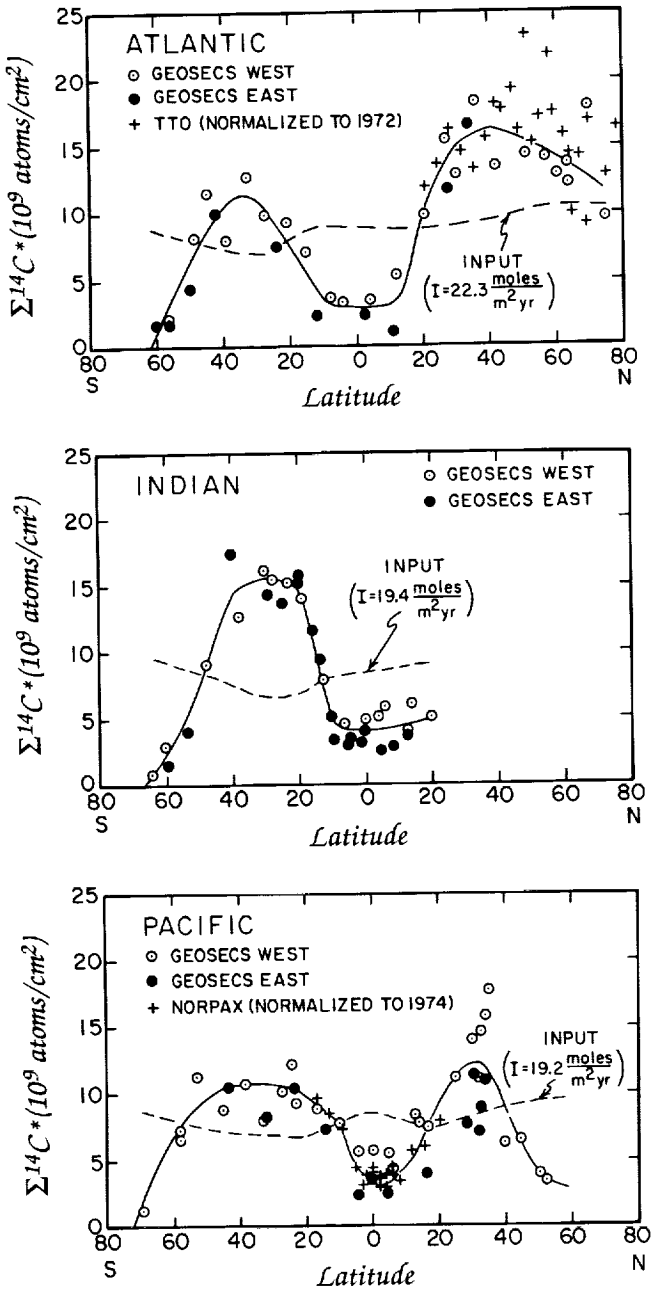

Figure 4. Bomb-produced ^{14}C inventories as measured during the GEOSECS, NORPAX, and TTO programs (as summarized by Broecker et al., 1985). The dashed lines show the amount expected at the time of the GEOSECS program were there no lateral transport from one zone to another. "I" represents CO_2 invasion rate.

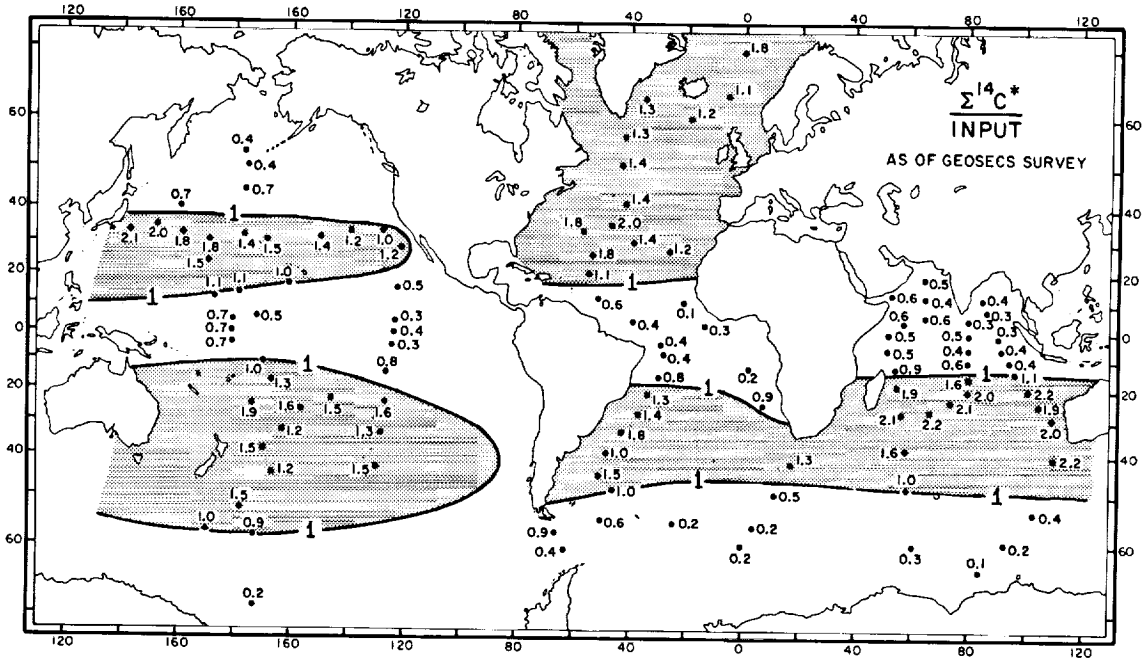

Figure 5. Map showing the ratios of observed bomb-testing radiocarbon inventories to those calculated were there no lateral transport (from Broecker et al., 1985).

calculations neglected the dependence of CO_2 exchange rate on wind speed. Were wind speed to be taken into account, the magnitude of the deficiencies for the Antarctic stations would be increased. The reason is that the wind speed and hence the CO_2 exchange rate over the Antarctic is higher than the global average. At all latitudes in the Antarctic, less bomb-produced ^{14}C is present than entered the ocean. The deficiencies range from very small at 45°S to as much as 90% of the total input closer to the Antarctic continent.

Together the ^{3}H penetration depths and the bomb-produced ^{14}C deficiencies allowed Broecker et al. (1985) to obtain estimates of the average upwelling and downwelling velocities for various regions of the ocean. The values they obtained are summarized in Table 2. For the Antarctic they require an average vertical eddy diffusivity of 3 cm^2/s and upwelling velocities ranging from 9 m/yr (for the Indian sector) to 31 m/yr (for the Atlantic sector).

Model of Antarctic and Non-Antarctic Oceans

Based on these tracer distributions and lateral transport mechanism of Broecker et al. (1985), we devised a box model of Antarctic and non-Antarctic oceans (Peng and Broecker, 1991a). It involves two, side-by-side, Oeschger et al. (1975) box-diffusion columns

Table 2: Comparison of surface water $\Delta^{14}C$ excesses and water column inventories of bomb-produced radiocarbon generated by the model of Broecker et al., 1985, with those observed GEOSECS.

Latitude Belt	Area (10^{12} m^2)	W[a] (m/yr)	Flux (Sv)	K[b] (cm^2/s)	z[c] (m)	$\Delta^{14}C - \Delta^{14}C^0$ (Modeled) (‰)	$\Delta^{14}C - \Delta^{14}C^0$ (Observed) (‰)	Bomb ^{14}C Input (10^{26} atoms)	Bomb ^{14}C Inventory (Modeled) (10^{26} atoms)	Bomb ^{14}C Inventory (Observed) (10^{26} atoms)
Atlantic (I[d] = 22.3 mol/m^2/yr)										
80°N–40°N	18.6	–8.5	5	9.9	710	130	120	20	26	26
40°N–20°N	15.8	–30.0	15	0.5	470	215	195	14	24	23
20°N–20°S	26.7	+21.2	18	1.0	190	146	150	25	11	10
20°S–45°S	18.4	–22.3	13	1.0	400	185	170	14	20	18
45°S–80°S	15.1	+31.2	15	3.0	270	100	100	14	6	7
Indian (I = 19.4 mol/m^2/yr)										
25°N–15°S	27.0	+15.2	13	1.0	215	130	160	26	11	12
15°S–45°S	29.8	–20.1	19	1.0	510	190	180	23	43	42
45°S–70°S	20.7	+9.1	6	3.0	410	115	100	19	14	13
Pacific (I = 19.2 mol/m^2/yr)										
65°N–40°N	15.1	+10.4	5	1.5	260	152	145	13	9	8
40°N–15°N	35.0	–10.8	12	1.0	365	206	210	30	39	37
15°N–10°S	50.0	+16.4	26	1.0	255	134	150	44	25	25
10°S–55°S	63.0	–12.5	25	2.0	410	166	170	48	64	60
55°S–80°S	13.8	+13.7	6	3.0	335	111	100	11	8	7

[a]W = upwelling rate
[b]K = vertical eddy diffusivity
[c]z = mean penetration depth, i.e., K/W
[d]I = CO_2 invasion rate
From Broecker et al., 1985

linked together by an overlying atmosphere and underlying deep sea (see Figure 6). One column represents the Antarctic and the other the non-Antarctic region of the ocean. Each column is capped by a 75-m-thick mixed layer. These mixed layers are underlain by 2000-

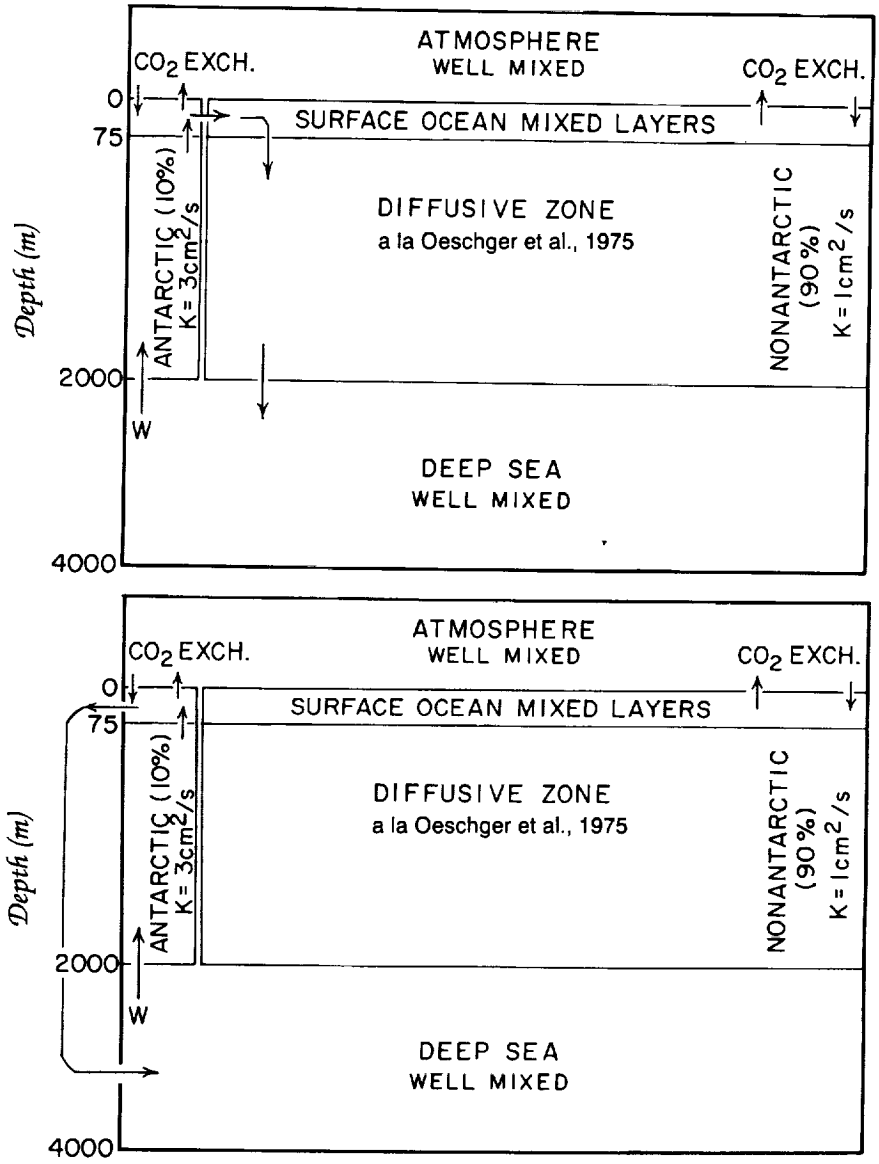

Figure 6. Linked vertical advection-diffusion model used to evaluate the response to iron fertilization of Antarctic surface waters. The upper panel shows the case where the water upwelled in the Antarctic is transferred laterally to the non-Antarctic surface ocean. The lower panel shows the case where this upwelled water is converted to deep water and transferred directly to the model's deep reservoir.

m-thick diffusive zones. Beneath the diffusive zone is a single well-mixed deep reservoir. The area and volume of the Antarctic column are taken to be 10% of the ocean total. We did not set the area of the Antarctic at 17% because iron fertilization could draw the surface water pCO_2 only during those months when sunlight is plentiful. In the light-poor austral winter months the pCO_2 would be driven back toward its prefertilization value by vertical mixing in the upper 100 m or so of the water column.

Consistent with the distribution of bomb radiocarbon, we set the vertical eddy diffusivity in the Antarctic column at 3 cm^2/s and that in the non Antarctic column at 1 cm^2/s. The upwelling flux in the Antarctic column was set at 17.4 Sverdrups (i.e., an upwelling rate of 15.2 m/yr). Because we had no firm means to determine the fate of the upwelled water, we adopted two limiting scenarios. In the first, all of the water is transferred entirely to the surface of the non-Antarctic column. In the second, it is transferred entirely to the deep reservoir.

We started our calculation with a steady state. The residence times for PO_4 with respect to biological removal from the surface reservoirs were set so as to yield 1.6 μmol PO_4 in the surface water above the Antarctic column and close to zero PO_4 in the surface waters of the non-Antarctic column. The regeneration function for falling organic debris was set to yield PO_4 vs. depth profiles similar to the observed (we hasten to point out that the choice of this respiration function has no influence on the result of the calculation of the atmospheric CO_2 response to iron fertilization). The atom ratio of carbon to phosphorus in the organic matter falling from the surface mixed layer is 130. We then adjusted the ΣCO_2/alkalinity ratio in the model ocean to yield an atmospheric pCO_2 pressure of 280 μatm.

To simulate a totally successful iron fertilization, we perturbed this steady state by greatly decreasing the residence time with respect to biological removal of PO_4 from Antarctic surface water, bringing its PO_4 content to near zero. In this simulation we continued the iron fertilization for 100 years, holding the PO_4 content of the surface Antarctic water at zero over this entire period. The evolutions of the vertical distributions of PO_4 and ΣCO_2 in the Antarctic column are shown in Figure 7. As can be seen, while the water column integral of PO_4 remains unchanged, a bulge of excess ΣCO_2 appears. This bulge represents the CO_2 transferred from the atmosphere and the non-Antarctic column to the Antarctic column (Peng and Broecker, 1991a). The time trends for the pCO_2 in the two ocean surface layers and in the atmosphere are shown in Figure 8. In the lateral transfer scenario, the atmospheric CO_2 content drops ever more slowly as the century progresses, reaching an asymptote about 15 μatm lower than the initial value. In the deep transfer sce-

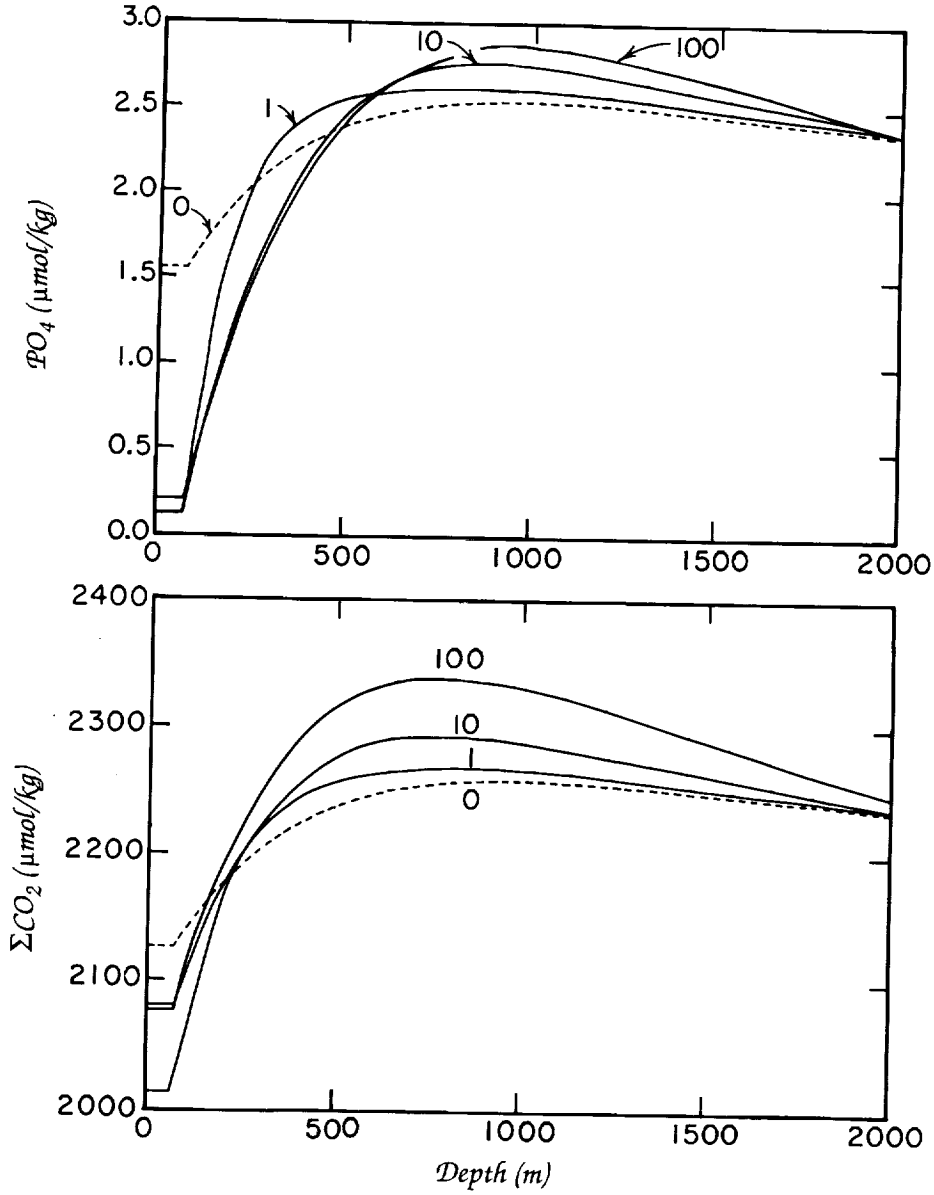

Figure 7. Vertical distribution of PO_4 and ΣCO_2 in the Antarctic column before the onset of fertilization (dashed line) and 1, 10, and 100 years after the onset of fertilization for the scenario where water is upwelled at the rate of 17.4 Sverdrups and transferred to the deep sea.

nario the decrease continues, reaching about 34 μatm after one century (Peng and Broecker, 1991a). The reason for the difference is that in one case the surface water from the Antarctic is transferred to the surface of the non-Antarctic region, allowing the excess CO_2

to reenter the atmosphere, while in the other this water is removed to the deep sea, isolating it from the atmosphere.

The question naturally arises as to what would happen if at some point iron fertilization were terminated. As shown in Figure 8, the answer is that any reduction in atmospheric CO_2 content accom-

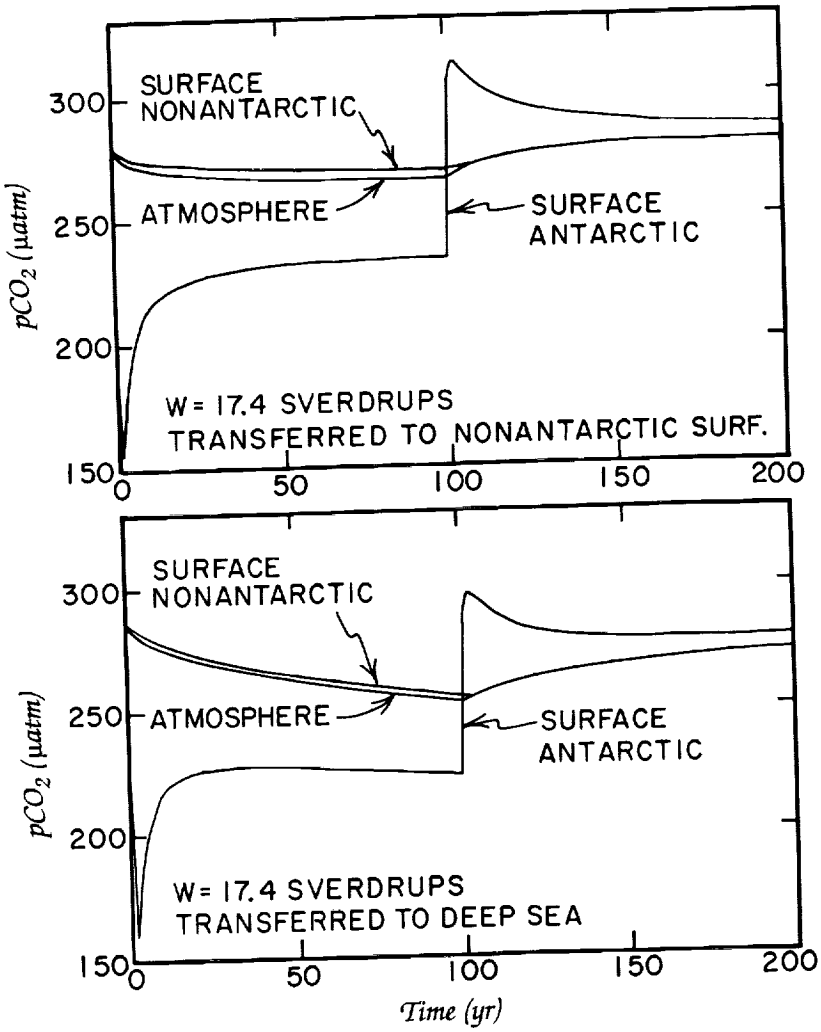

Figure 8. Model runs for an Antarctic upwelling flux of 17.4 Sverdrups. The upper panel shows the case where the upwelled water is transferred to the surface of the non-Antarctic Ocean; the lower panel shows the case where the upwelled water is transferred to the deep sea. In each case totally successful iron fertilization is conducted for 100 years and then stopped. For the steady state conditions which precede the onset of fertilization, the pCO_2 for Antarctic surface waters is nearly identical to that for the atmosphere.

C-2

plished by the fertilization would be lost on more or less the same time scale as it was gained.

As a sensitivity test, we have made runs for upwelling fluxes of twice and half the 17.4 Sverdrups value for our best case scenario and also for no advection. As summarized in Table 3, changes in upwelling flux have little effect on the results for the lateral transport endmember model. However, in the case of the deep transfer endmember model, the greater the upwelling flux, the greater the reduction of the atmospheric CO_2 content brought about by iron fertilization. Clearly, the key question to be answered in the evaluation of the dynamic constraints on the iron fertilization scheme is the rate and extent of vertical transport in the Antarctic.

Effects on an Anthropogenically Affected Atmosphere

To test the effects of iron fertilization on an anthropogenically affected atmosphere, we introduced excess CO_2 into the atmosphere starting in 1800 and continuing through 1990. The input function of fossil fuel production was based on a recent estimate (Marland, 1990). The release of CO_2 from the perturbed terrestrial ecosystem was derived from deconvolution (Peng, 1991) of the time history of atmospheric pCO_2 based on pCO_2 measurements of air bubbles in ice cores (Neftel et al., 1985) and of air samples (Keeling et al., 1989). The release scenario of the business-as-usual case for the next century was taken from a report of the Intergovernmental Panel on Climate Change (IPCC; Houghton et al., 1990). The CO_2 emission between 1800 and 2100 is shown in Figure 9. Before introducing anthropogenic CO_2, the steady state of our ocean-atmosphere model with pCO_2 of 280 µatm was the same as described earlier. Shown in Figure 10 is the atmospheric pCO_2 for the next century resulting from the

Table 3: Summary of pCO_2 after 100 years of iron fertilizaiton

Experiment No.	Upwell Rate (sv)	pCO_2 initial Atm. (µatm)	pCO_2 final Atm. (µatm)	pCO_2 final non-Ant. (µatm)	pCO_2 final Ant. (µatm)	ΔpCO_2 Atm. (µatm)
1	34.8	280.5	265.5	270.8	215.2	-15.0
2	17.4	279.7	265.0	268.5	232.2	-14.7
3	8.7	280.0	263.2	265.6	240.1	-16.8
4	0.0	284.3	262.2	263.2	248.2	-22.1
5	8.7*	283.1	255.2	256.8	233.4	-27.9
6	17.4*	286.0	251.6	253.7	221.7	-34.4
7	34.7*	291.0	244.0	246.8	200.7	-47.0

*The water upwelled in the Antarctic is converted to deep water.

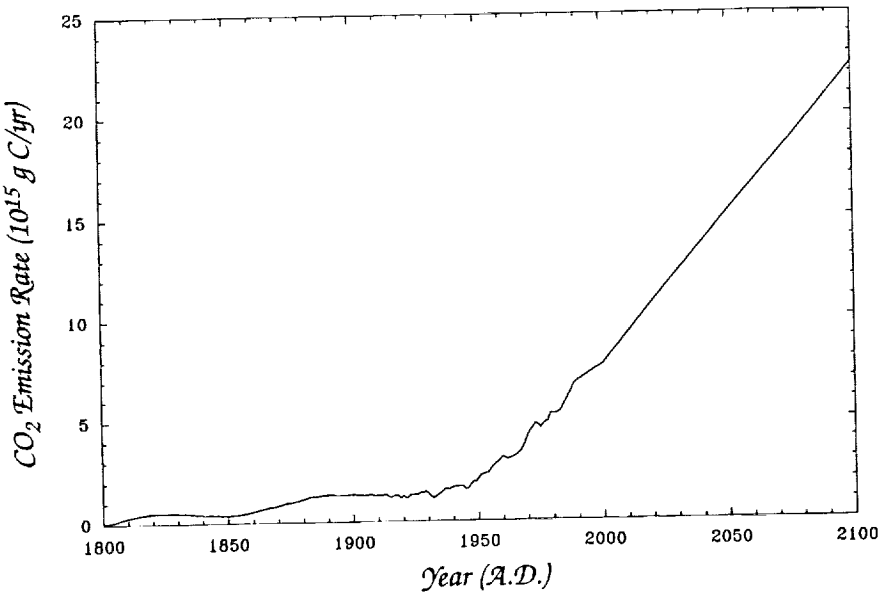

Figure 9. Time history of CO_2 emission for the period between 1800 and 1990 combined with the IPCC business-as-usual CO_2 release scenario for the period between 1991 and 2100.

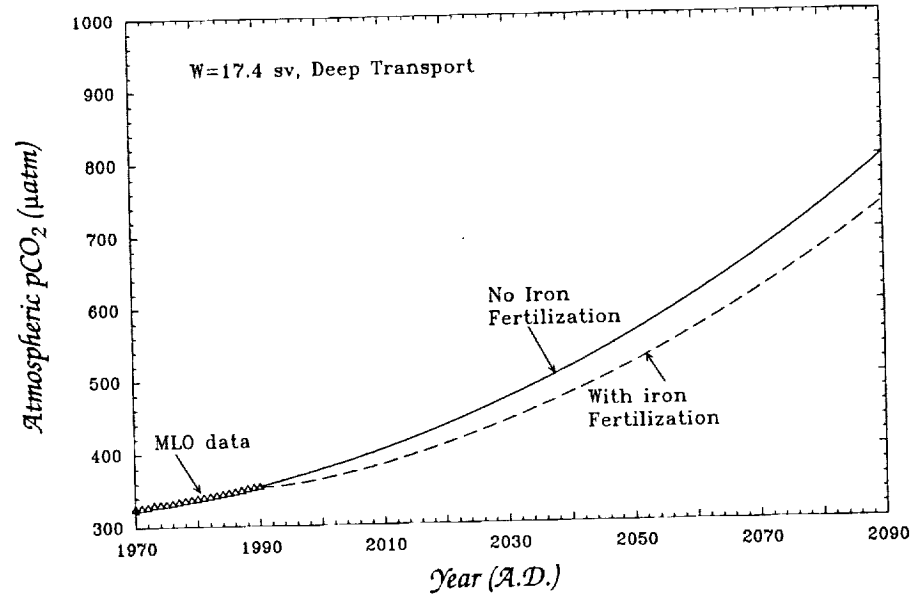

Figure 10. Atmospheric pCO_2 from Mauna Loa Observatory measurements (1970–1990) combined with the IPCC business-as-usual CO_2 emission scenario (1991–2090). The solid curve is the predicted atmospheric pCO_2 without iron fertilization, and the dashed curve is the one with iron fertilization in the Antarctic Ocean. Standard dynamic conditions of 17.4 sv upwelling flux and deep transport of upwelled water are used for simulation.

IPCC CO_2 release scenario without iron fertilization in the Antarctic Ocean. An upwelling flux of 17.4 sv is used, and the upwelled water is transferred to the deep reservoir. The result of a successful iron fertilization to reduce the atmospheric pCO_2 under such dynamic conditions is also shown in the same figure for comparison. The difference between these two curves represents the net effect of iron fertilization.

We made a series of sensitivity calculations with various upwelling fluxes to estimate the amount of reduction in atmospheric pCO_2 with 100% successful iron fertilization in the Antarctic. As shown in Figure 11, the lateral transport scenario is not sensitive to upwelling fluxes, with reductions in the range of 20 to 30 μatm for the time in the next century when the atmospheric pCO_2 reaches 800 μatm. This reduction corresponds to only about 3% of the atmospheric CO_2 content. But, in the case of deep transport, the reduction is very sensitive to upwelling fluxes. The reduction ranges from 6% of the atmospheric pCO_2 for an 8.7-sv upwelling flux to 12% for a 34.8-sv upwelling flux, with the best case of 8% reduction (or 64 μatm) for a 17.4-sv upwelling flux.

Similar model simulations of the possible effects of iron fertilization in the Southern Ocean on atmospheric pCO_2 have been made by Joos et al. (1991a, 1991b). Their model is a high-latitude exchange and low-latitude interior diffusion advection four-box model calibrated with bomb ^{14}C distribution. The Antarctic Ocean is represented by two well-mixed boxes, one for the surface and one for deep water. They obtained a reduction of 107 μatm for the IPCC business-as-usual release scenario under their standard dynamic condition after 100 years of successful iron fertilization in the Antarctic. Their sensitivity tests showed that the most important factors affecting the magnitude of CO_2 reduction are the area of fertilization and the amount of future CO_2 emissions.

The lower estimates of atmospheric pCO_2 reduction in our simulations as compared with those of Joos et al. (1991a, 1991b) have been criticized as resulting from the failure of our model to use a larger surface area for fertilization (i.e., 16%, instead of 10%). However, as reported by Peng and Broecker (1991b), a reduction of 71 μatm after 100 years of successful iron fertilization is estimated if the total Antarctic surface area is taken to be 16% of the global ocean area. This estimate is not significantly different from a reduction of 64 μatm in the standard case. The reason for such a small difference is that the upwelling flux of 17.4 sv is kept constant in spite of increased surface area. It was the upwelling flux rather than an upwelling rate that was constrained by Broecker et al. (1985) in their analysis of the bomb ^{14}C data. The increase in surface area causes the upwelling rate to drop from 15.2 to 9.5 m/yr.

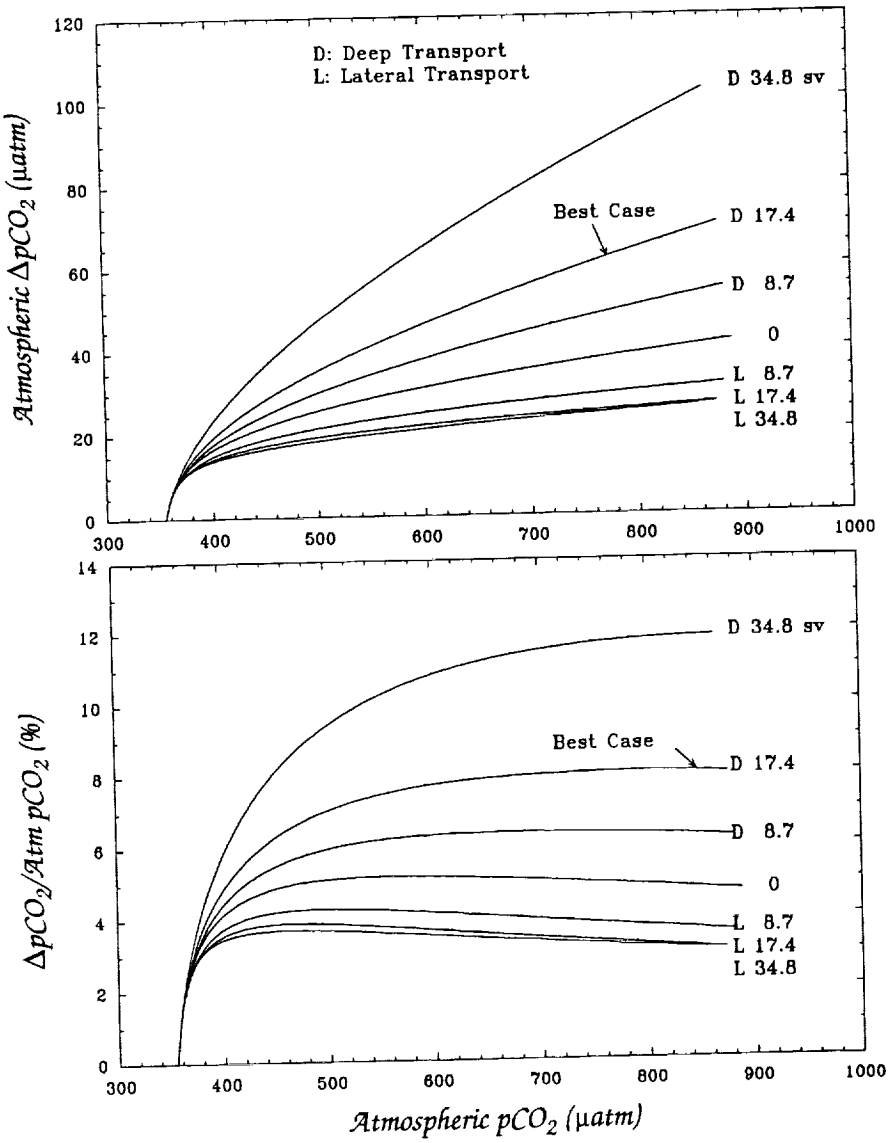

Figure 11. Reduction in pCO_2 in the atmosphere with iron fertilization in the Antarctic ocean for the period between 1991 and 2100 when the release of anthropogenic CO_2 into the atmosphere is taken from the IPCC business-as-usual case. Magnitude of reduction is plotted against the atmospheric pCO_2 in the upper panel, while the percentage of reduction is plotted in the lower panel.

More elaborate model simulations were made by Sarmiento and Orr (in press) using a three-dimensional ocean carbon cycle model based on a general circulation model (GCM). A reduction of 72 μatm in the next 100 years was obtained for a successful iron fertilization in the Southern Ocean (with 16% surface area) when the anthropogenic CO_2 emission followed the IPCC business-as-usual scenario. It is interesting to note that our estimate is comparable with theirs, although there are large differences in the modeling approaches.

Effects of Seasonal Iron Fertilization

Light availability certainly limits photosynthesis in the Antarctic, especially during the winter months. To gain some idea regarding the impact of this limitation, we have introduced seasonality into our model. It involves turning off the impact of iron fertilization for a number of months each year. We do this without changing the model's dynamics: i.e., upwelling and vertical mixing continue unchanged throughout the year. Shown in Figure 12 are the resulting surface water PO_4 and pCO_2 cycles for the first four years after the onset of fertilization for the scenario involving 17.4 sv upwelling coupled with transport to the deep sea. The period of totally successful fertilization is set at eight, four, and two months. These results depend strongly on our choice of PO_4 residence time in the mixed layer during the period of fertilization and on the choice of vertical eddy diffusivity. Our choices lead to a rapid drawdown of phosphate content of the mixed layer after the onset of fertilization, but much slower rise when fertilization ceases. Under these circumstances four winter months of no productivity caused only a small reduction in the long-term CO_2 drawdown (see Figure 13). Even when the period of fertilization was reduced to only two months per year, two-thirds of the atmospheric CO_2 drawdown achieved for the full-year scenario occurred (see Figure 13).

It is tempting to conclude from this that were iron added for only two months of the year, two-thirds of the maximum possible atmospheric drawdown would be achieved. We urge caution in this regard; our result depends very strongly on the ratio of the PO_4 drawdown time to the water replacement time for the mixed layer. Were a less favorable ratio to be adopted, the turnoff of iron fertilization would have more nearly a proportional impact. Our choice of one month for the phosphate drawdown time is just a guess. As our surface water replacement time is chosen to match the vertical distribution of tritium about one decade after the cessation of large-scale bomb testing, it has little bearing on the actual rate of water exchange

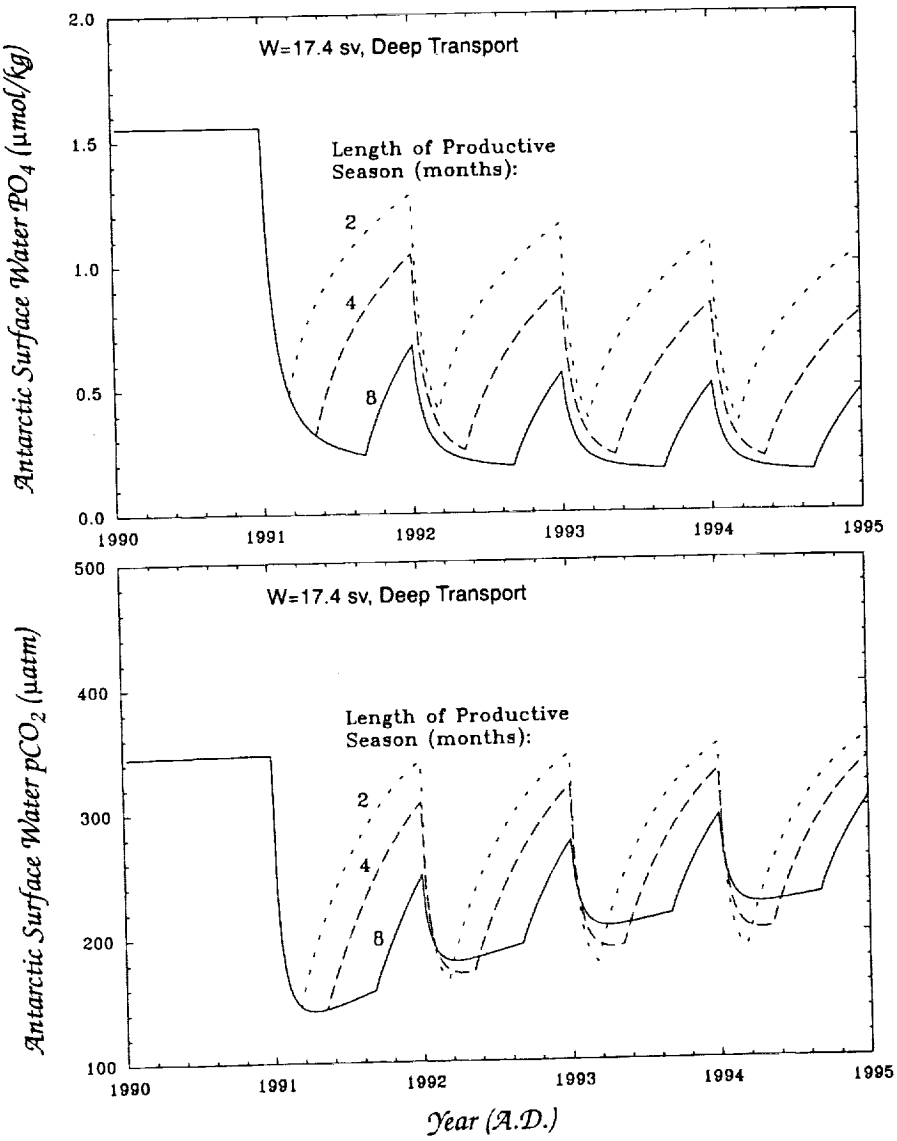

Figure 12. Seasonal cycles of surface water pCO_2 and PO_4 in the Antarctic with a productive season of eight months (solid line), four months (long dashed line), and two months (short dashed line). Iron fertilization is assumed to work successfully during the productive season. The PO_4 cycle is plotted in the upper panel for the first four years after the fertilization, and the pCO_2 cycle is plotted in the lower panel.

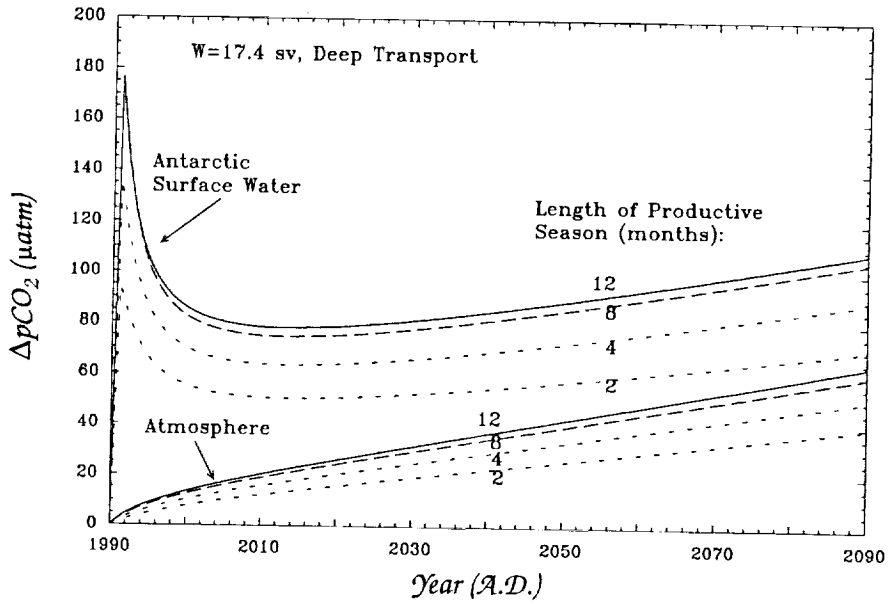

Figure 13. Reduction of pCO_2 in the atmosphere and in the Antarctic surface water resulting from seasonal iron fertilization. A two-thirds total reduction in the atmosphere can be achieved by two-twelfths yearly fertilization with iron in the Antarctic Ocean.

between the mixed layer and the underlying thermocline. Further, the actual vertical exchange has a strong seasonality. Winter cooling thickens the mixed layer, while summer warming and sea ice melting thin it. The only valid conclusion to be drawn from our seasonality exercise is that careful attention should be given to seasonality in any plan for iron fertilization. The interplay of changing light availability and vertical mixing with the timing of iron addition could be used to optimize the amount of atmospheric CO_2 drawdown per unit fertilization cost.

Implications of SAVE ^{14}C Results

The real power of transient tracer data is seen when the spatial distribution is used in combination with temporal evolution. Unfortunately, no more recent tritium and ^{14}C data sets are available. However, ^{14}C data have recently become available from four stations occupied during the South Atlantic Ventilation Experiment (SAVE) survey of the South Atlantic (see Figure 1 for locations). Two of these stations are close to GEOSECS station 68 at the northern fringe of the Antarctic in the Argentine Basin. While the depth profiles of ^{14}C at these stations are quite different than that at station 68, when ^{14}C is plotted against silica absolutely no difference is seen (Figure 14). This is puzzling because the silica distribution is at steady state

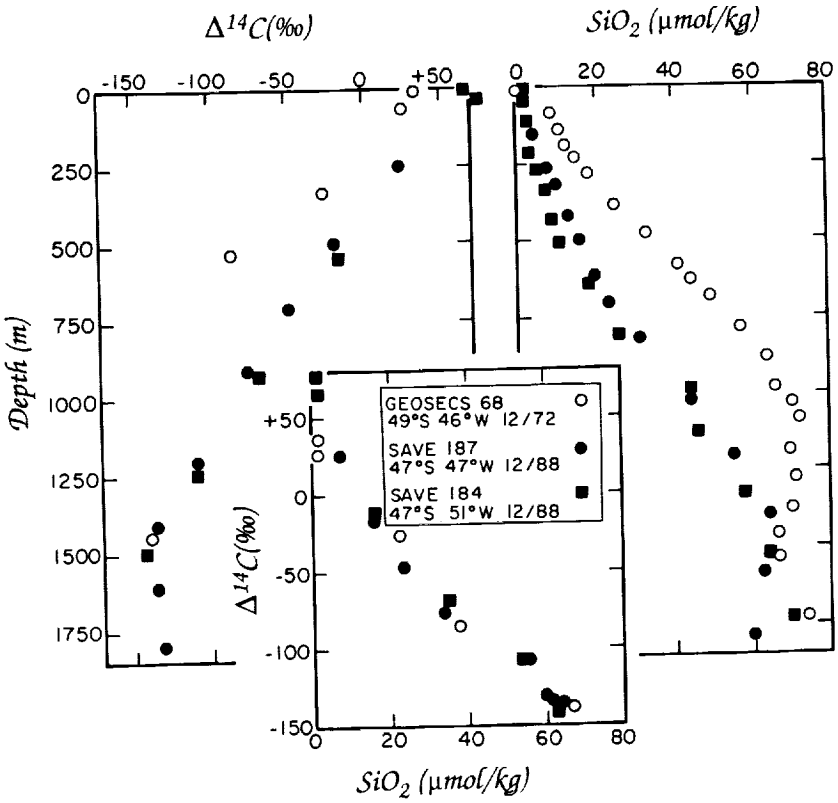

Figure 14. Comparison of depth profiles for silica and radiocarbon and of silica vs. radiocarbon trends for GEOSECS station 68 (December 1972) and nearby SAVE stations 184 and 187 (December 1988). As can be seen, the relationship between radiocarbon (a transient) and silica (at steady state) shows no change over this period of time. The 1988 silica results are from the SAVE preliminary data report series and the 1988 radiocarbon results are from Östlund, 1990.

while the ^{14}C distribution is evolving. The other two recent stations lie within the Antarctic. As can be seen in Figure 15, again no change in the ^{14}C-silica trend is seen over a 16-year period. One gets the idea that the vertical distribution of bomb-produced ^{14}C adjusted to a transient steady state on a time scale of a decade and that as the surface water $\Delta^{14}C$ value went up and then came back down again (see Figure 16) in response to the changing atmospheric $\Delta^{14}C$, the Antarctic $\Delta^{14}C$-silica trend rotated first toward a higher $\Delta^{14}C$ value and then back down again, reaching by chance its December 1972 value once again in December 1988 during SAVE survey.

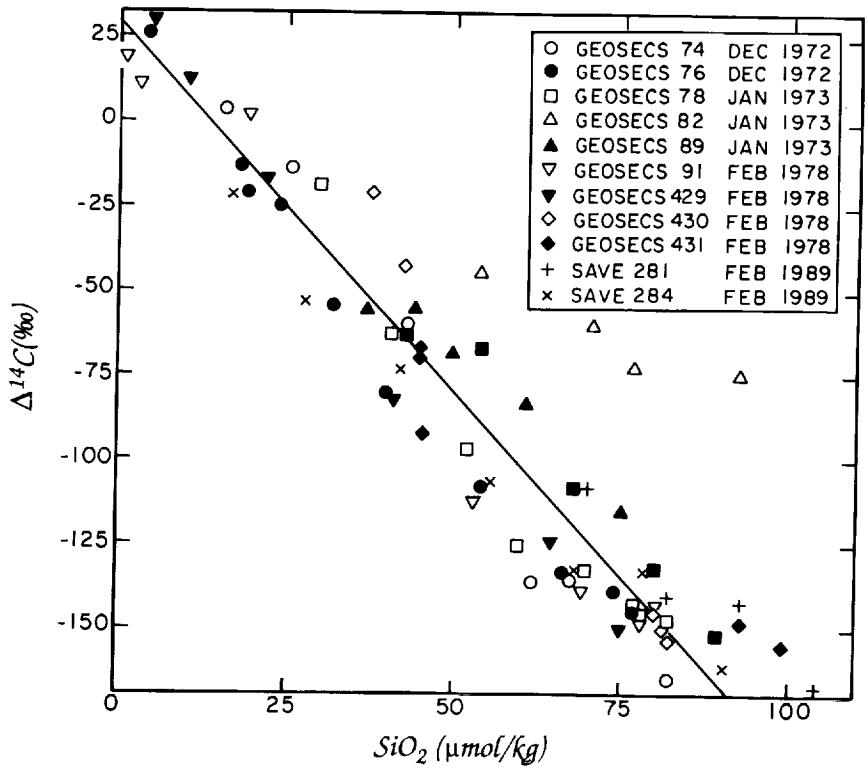

Figure 15. Relationship in the Antarctic between radiocarbon and silica for the GEOSECS Atlantic stations, three of the GEOSECS Indian stations, and two SAVE stations. Despite the passage of 16 years from late 1972, when the GEOSECS Atlantic samples were taken, to early 1989, when the SAVE samples were taken, no evidence exists for a change in the radiocarbon-silica relationship. Only the GEOSECS station (82) which is the nearest to the Weddell Sea departs from the ambient trend. It should be kept in mind that prior to bomb testing no waters in the Antarctic had ^{14}C values above −75‰. The GEOSECS data are from sources mentioned above and the SAVE data are from the preliminary shipboard measurement report and from Östlund, 1990.

As can be seen in both Figures 14 and 15, no evidence exists for a buildup of bomb ^{14}C in waters with more than about 80 µmol of silica. The ^{14}C content of these waters lies close to the average (see Figure 17) obtained by GEOSECS for deep waters of the Antarctic (potential temperatures in the range of 0 to 1°C). Hence, little excess CO_2 entering the Antarctic as the result of iron fertilization can be expected to reach waters with more than 80 µmol of silica on a time scale of 25 years. A sense of magnitude of the volume of water lying above this silica horizon is shown in Figure 3.

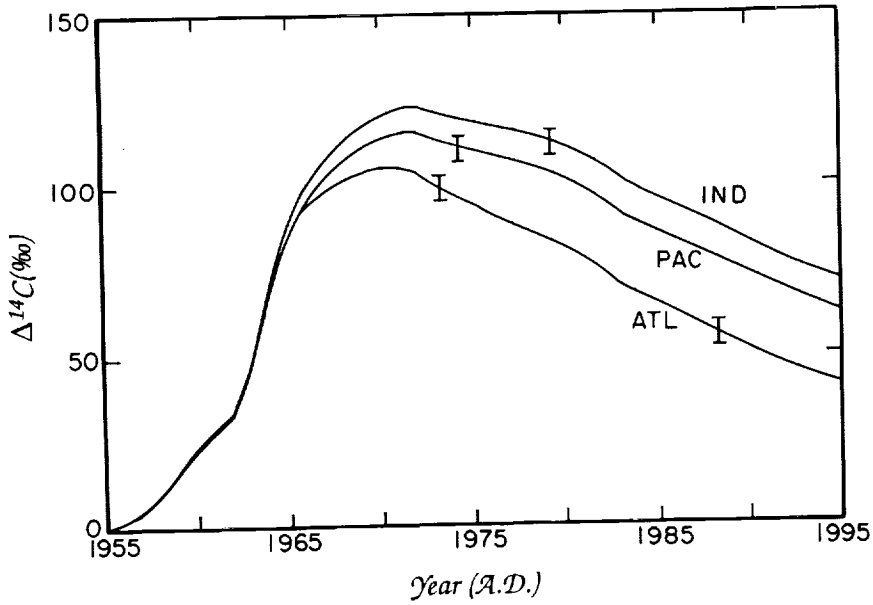

Figure 16. Time trends for the surface water ^{14}C computed using the Broecker et al. (1985) column models for three sectors of the Antarctic. The times for the GEOSECS and SAVE sampling are marked with hashes.

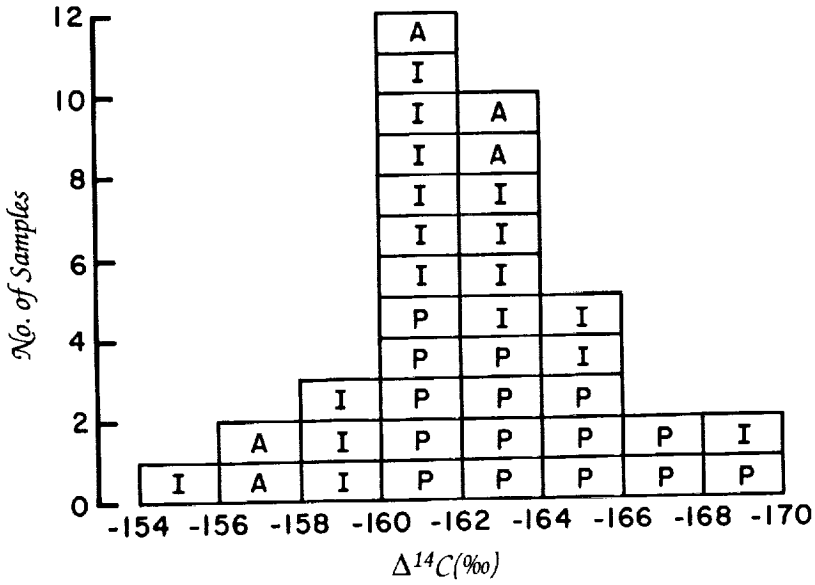

Figure 17. Summary of GEOSECS results on deep water samples from the Antarctic (Östlund and Stuiver, 1980; Stuiver and Östlund, 1980; Stuiver and Östlund, 1983). A represents Atlantic, P represents Pacific, and I represents Indian.

Conclusion

While our ability to model what goes on in the Antarctic remains in a primitive state, the evidence we have certainly waves a red flag with regard to optimistic claims (see Baum, 1990) that iron fertilization of the Antarctic, even if biologically successful, will significantly draw down the CO_2 content of the atmosphere. Interest in this possible intervention scenario clearly adds yet another item to an already long list of reasons why we should redouble our efforts to obtain extensive transient tracer data for the Antarctic.

Acknowledgments

Discussion with J. Sarmiento prompted this study. Modeling of bomb radiocarbon transient in an ocean GCM by R. Toggweiler rekindled our thinking about tracers in the Antarctic. Financial support was provided by grants from the Exxon Corporation and the Carbon Dioxide Research Program, Environmental Sciences Division, Office of Health and Environmental Research, U.S. Department of Energy, under contract DE-AC05-84OR21400 with Martin Marietta Energy Systems, Inc. This chapter is publication No. 3744, Environmental Sciences Division, Oak Ridge National Laboratory, and contribution No. 4828, Lamont-Doherty Geological Observatory of Columbia University.

References

Baum, R. 1990. Adding iron to ocean makes waves as way to cut greenhouse CO_2. *Chemical & Engineering News*, July 2, 1990, 21–24.

Broecker, W.S., T.-H. Peng, G. Östlund, and M. Stuiver. 1985. The Distribution of bomb radiocarbon in the ocean. *Journal of Geophysical Research 90*, 6953–6970.

Broecker, W.S., T.-H. Peng, and G. Östlund, 1986. The distribution of bomb tritium in the ocean. *Journal of Geophysical Research 91*, 14331–14344.

Houghton, J.T., G.J. Jenkins, and J.J. Ephraums (eds.). 1990. *Climate Change: The IPCC Scientific Assessment.* Intergovernmental Panel on Climate Change and Cambridge University Press, Cambridge, 329–341.

Joos, F., J.L. Sarmiento, and U. Siegenthaler. 1991a. Potential enhancement of oceanic CO_2 uptake by iron fertilization of the Southern Ocean. *Nature 349*, 772–775.

Joos, F., U. Siegenthaler, and J.L. Sarmiento. 1991b. Possible effects of iron fertilization in the Southern Ocean on atmospheric CO_2 concentration. *Global Biogeochemical Cycles 5*, 135–150.

Keeling, C.D., R.B. Bacastow, A.F. Carter, S.C. Piper, T.P. Whorf, M. Heimann, W.G. Mook, and H. Roeloffzen. 1989. A three-dimensional model of atmospheric CO_2 transport based on observed winds: 1. Analysis of observational data. In *Climate Change in the Eastern Pacific and Western Americas* (D. Peterson, ed.), Geophysical Monographs 55, American Geophysical Union, Washington, D.C., 165–231.

Marland, G. 1990. Global CO_2 emissions. In *Trends '90: A Compendium of Data on Global Change* (T.A. Boden, P. Kanciruk, and M.P. Farrell, eds.), ORNL/CDIAC-36, Carbon Dioxide Information Analysis Center, Oak Ridge National Laboratory, Oak Ridge, Tennessee, 92.

Martin, J.H. 1990. Glacial-interglacial CO_2 change: The iron hypothesis. *Paleoceanography 5*, 1–13.

Martin, J.H., and S.E. Fitzwater. 1988. Iron deficiency limits phytoplankton growth in the northeast Pacific subarctic. *Nature 331*, 341–343.

Martin, J.H., and R.M. Gordon. 1988. Northeast Pacific iron distributions in relation to phytoplankton productivity. *Deep Sea Research 35*, 177–196.

Martin, J.H., R.M. Gordon, S. Fitzwater, and W.W. Broenkow. 1989. VERTEX: Phytoplankton/iron studies in the Gulf of Alaska. *Deep-Sea Research 36*, 649–680.

Martin, J.H., R.M. Gordon, and S. Fitzwater. 1990a. Iron in Antarctic waters. *Nature 345*, 156–158.

Martin, J.H., S.E. Fitzwater, and R.M. Gordon. 1990b. Iron deficiency limits phytoplankton growth in Antarctic waters. *Global Biogeochemical Cycles 4*, 5–12.

Neftel, A., E. Moor, H. Oeschger, and B. Stauffer. 1985. Evidence from polar ice cores for the increase in atmospheric CO_2 in the past two centuries. *Nature 315*, 45–47.

Östlund, H.G. 1990. South Atlantic Ventilation Experiment (SAVE) Radiocarbon results, Legs 4,5 and Hyrdos Leg 4. University of Miami Report.

Östlund, H.G., and M. Stuiver. 1980. GEOSECS Pacific radiocarbon. *Radiocarbon 22*, 25–53.

Oeschger, H., U. Siegenthaler, U. Schotterer, and A. Gugelman. 1975. A box diffusion model to study the carbon dioxide exchange in nature. *Tellus 27*, 168–192.

Peng, T-H. 1991. Oceanic CO_2 uptake and future atmospheric CO_2 concentrations. In *Air-Water Mass Transfer: Selected Papers from the Second International Symposium on Gas Transfer at the Water Surfaces* (S.C. Wilhelms and A.J. S. Gulliver, eds.). American Society of Chemical Engineers, New York, 618–636.

Peng, T.-H., and W.S. Broecker. 1991a. Dynamic limitations on the Antarctic iron fertilization strategy. *Nature 349*, 227–229.

Peng, T.-H., and W.S. Broecker. 1991b. Factors limiting the reduction of atmospheric CO_2 by iron fertilization. *Limnology and Oceanography 36(8)*, 1919–1928.

Sarmiento, J.L., and J.C. Orr. Three dimensional ocean model simulations of the impact of Southern Ocean nutrient depletion on atmospheric CO_2 and ocean chemistry. *Limnology and Oceanography*, in press.

Stuiver, M., and H.G. Östlund. 1980. GEOSECS Atlantic radiocarbon. *Radiocarbon 22*, 1–24.

Stuiver, M., and H.G. Östlund. 1983. GEOSECS Indian Ocean and Mediterranean radiocarbon. *Radiocarbon 25*, 1–29.

Sverdrup, H.U., M.W. Johnson, and R.H. Fleming. 1942. *The Oceans, Their Physics, Chemistry and Biology*, Prentice-Hall, Englewood Cliffs, New Jersey.

Toggweiler, J.R., K. Dixon, and K. Bryan. 1989. Simulations of radiocarbon in a coarse-resolution world ocean model: 2. Distributions of bomb-produced carbon 14. *Journal of Geophysical Research 94*, 8243–8264.